PCCP

Accepted Manuscript

ROYAL SOCIETY OF CHEMISTRY

www.rsc.org/pccp

Electromagnetic interference shielding in 1-18 GHz frequency and electrical properties correlations in poly(vinylidene fluoride)-multi-walled carbon nanotube composites

*G. Sudheer Kumar[1], Vishnupriya D.[1], Anupama Joshi[2], Suwarna Datar[2] and T. Umasankar Patro[1]**

[1]Department of Materials Engineering, Defence Institute of Advanced Technology, Girinagar, Pune 411025, India.

[2]Department of Applied Physics, Defence Institute of Advanced Technology, Girinagar, Pune 411025, India.

ABSTRACT:

Electromagnetic interference (EMI) shielding properties in 1-18 GHz frequency range for multi-walled carbon nanotube (MWNT)-poly(vinylidene fluoride) (PVDF) composites are reported. A simple and gentle acid-treatment of MWNT showed a percolation threshold (PT) of 0.15wt% in PVDF matrix as against 0.35wt% for unfunctionalized MWNT. Acid-treatment of MWNT significantly improves dispersion, interfacial adhesion with matrix and the EMI shielding properties of PVDF composites. Further, the EMI shielding properties are correlated with the electrical properties. Using composite films of 0.3 mm thick, the maximum shielding effectiveness (SE_T) values for 4wt% unfunctionalized MWNT composites are found to be about 110, 45, 30, 26, 58 dB for L (1-2 GHz), S (2-4 GHz), C (4-5.8 GHz), J (5.8-8 GHz), X (8-12 GHz) bands; while the corresponding values for only 0.5wt% acid functionalized MWNT composites are about 98, 45, 26, 19, and 47 dB, respectively. The electrical conductivity for both the cases is ~10^{-3} S/cm and the weight contents of CNTs are higher than the PT for the respective composites. The comparable EMI SE and electrical conductivity values for both the composites at different weight fractions of CNTs suggests that there is a critical electrical conductivity above which the composites attain improved EMI shielding properties. Further, the shielding mechanism was found to be dominated by absorption loss. Therefore, the composites may also serve as a radar absorbing material.

KEYWORDS: Multi-walled carbon nanotubes, poly(vinylidene fluoride), shielding effectiveness, percolation threshold, electrical properties, absorption loss.

1. INTRODUCTION

In recent years, the field of electronics and communication has witnessed a rapid growth in terms of development of advanced technologies and products; like, cellular phones, high speed communication systems, military wireless devices, advanced radars etc., to name a few. Electromagnetic interference (EMI) is an undesirable phenomenon which significantly affects the performance of the modern devices and causes signal loss in communication. Further, studies revealed that exposure of electromagnetic waves for prolonged period poses health hazards to the human life.[1,2] Therefore, a considerable research effort has been put in developing cost effective and light-weight EMI shielding materials in recent past in order to minimize the EMI.[2-5] Modern communication devices work in a wide frequency range, which comprises various EM bands. These EM bands have different applications. For example, L band (1-2 GHz) is used by low earth orbit satellites, wireless communication etc.; S band (2-4 GHz) in multi media applications like mobile, TV, cordless phones and so on; C band (4-5.8 GHz) finds applications in long distance radio telecommunication, Wi-Fi devices; X-band (8-12 GHz) is generally used for weather monitoring, air traffic control, defence tracking and Ku (12-18 GHz) band is used by very small aperture terminal systems.[6,7]

EMI shielding is a material property that can attenuate EM waves either by reflection and/or by adsorption.[5] The reflection occurs due to impedance mismatch between ambient (incident wave) and shielding material[8]. Hence the shield is required to have mobile charge carriers in order to interact with the EM waves. For absorption loss, the shield should have nomadic charge carriers and/or electric or magnetic dipoles that interact with the EM field in the radiation.[9,10] The electric and magnetic dipoles are provided by the materials having high values of dielectric constant and magnetic permeability, respectively.[5]

Owing to their good electrical conductivity, metals have been traditionally used as EMI shielding materials.[11] However, they suffer from poor chemical resistance, corrosion, high density and difficulty in processing. Polymer composites with carbon based fillers could be potential replacements for conventional materials as EMI shielding materials due to their unique combination of light-weight and mechanical, electrical and thermal properties. Amongst various carbon based conducting composites; *viz.*, carbon nanotubes (CNTs),[3,12-19] graphite,[20] carbon black,[21-23] carbon fibres[24,25] and graphenes,[26,27] CNT composites have shown promising EMI shielding properties due to their good electrical properties and large aspect ratio.[3,12-19,28] Above electrical percolation threshold (PT), CNTs impart conductivity by creating a three dimensional interconnecting network in polymer matrix. Besides, these composites exhibit excellent EMI shielding properties; hence, probably most studied in the literature.[3,12-15,17-20,28-39] Here we present a brief overview of some important studies reported on polymer based composites for EMI shielding applications.

Sharma et al.[5] reported maximum EMI shielding effectiveness (SE) of ~31 dB for both PVDF composites with 3wt% CNTs and composite with 3wt% CNT and 5vol% graphene oxide grafted barium titanate nanoparticles (BT-GO) between 8 and 18 GHz frequency range. When the composites were made with 3wt% CNT along with 2.2vol% of cobalt nanowires (CoNWs), the SE showed a marginal increase to ~35 dB from ~31 dB for PVDF-3wt% CNT composites. The above fillers; *viz.*, BT-GO and CoNWs were used in order to improve the dielectric permittivity and magnetic permeability of CNT composites, respectively.[5] In another study, Sharma et al.[40] studied SE of ionic liquid modified CNTs (IL-MWNT) and PVDF composites in the frequency range of 8-18 GHz and obtained a SE of 20 dB with 2wt% of IL-MWNTs. Eswaraiah et al.[41] found the SE of ~20 dB and ~18 dB in X-band and in 1-8 GHz frequency

range, respectively, for PVDF foam with 5wt% of functionalized graphene. Rath et al.[42] found a reflection loss of ~37 dB in 6-12 GHz frequency for PVDF composites with 0.25wt% CNT using a ~25 μm thick film. He et al.[43] studied microwave absorption properties of CuS nanoparticles and PVDF composites in the frequency range of 2-18 GHz with films of different thicknesses. They obtained a maximum reflection loss of ~102 dB at 7.7 GHz in a 3.5 mm thick composite film with 5wt% CuS and higher CuS weight fractions (10 and 15wt%) did not improve the reflection losses. Further the reflection loss was found to be highly frequency dependent and showed large variations with frequency.[43] Sundararaj et al.[30] reported SE of ~36 dB in X-band for 1 mm thick sheet made of MWNT (7.5vol%)-polypropylene composite. Yang et al.[31] achieved SE of ~20 dB in composites of polystyrene with 7wt% MWNT in X-band. Further, studies have shown that higher CNT loading in polymer led to significant trade-off in mechanical properties.[16,44] Moreover, high weight fractions of CNTs were not found to increase the SE to a high value.[32,33] For instance, Liu et al.[32] achieved only ~17 dB SE in a 2mm thick film of 20wt% SWNT-polyurethane composites in X-band and Kim et al.[33] reported ~27 dB SE with 40wt% of MWNT loading in poly(methyl methacrylate) in the frequency range of 0.05-13.5 GHz using 60-165 μm thick films. Other fillers, like carbonyl iron powder at high weight faction, i.e., 50vol% in PVDF matrix showed only SE of 20 dB.[45]

A common observation emerged from the various reported studies is that there is a considerable scatter in the EMI shielding properties in terms of shielding effectiveness, even for two similar composite systems. Further, few studies have reported the EMI shielding properties in 1-18 GHz range for CNT composites, which covers a wide range of EM bands (from L to Ku band).[41,46,47] Most of the studies focus on X and Ku bands,[5,17,21,34,40,41,48-56] likely due to their wide application and requirement of small specimen size. Furthermore, a significant complexity

in composite preparation has also been observed in terms of functionalization of CNTs and use of surfactants and other nanofillers etc., in order to improve the EMI shielding properties.[5,40,57] Moreover, the role of PT and electrical conductivity in determining the EMI shielding properties is not well understood. We attempted to address these issues by choosing a simpler composite system comprising PVDF and MWNTs (both pristine and dilute nitric acid-treated CNTs). The gentle acid-treatment removed impurities from CNTs and resulted in weak oxidation. Because of this, the acid-treated CNTs showed low PT, better dispersion and interfacial adhesion with polymer matrix. Further, the MWNTs used in the present study were low-cost industrial grade CNTs, which may make the composites cost-effective for EMI shielding.

PVDF, a semicrystalline thermoplastic fluoropolymer, is known to possess a good acid and solvent resistance properties, high thermal stability, good mechanical properties and also it possesses a good ferroelectric, piezoelectric and pyroelectric properties.[40,43] PVDF has diversified applications; such as coating material in modern buildings, sensors, batteries, in ultrapure environments etc. Further, recently, PVDF composites were prepared with a wide range of nanoparticles for EMI shielding applications.[3-5,40-43] Further, PVDF, which contains electrophilic fluorine atoms in its chemical structure, is likely to have a better interaction with CNTs.

In the present work, we have investigated the EMI shielding properties of PVDF/MWNT composites in the frequency range of 1-18 GHz. Two varieties of CNTs; *viz.*, pristine (uf-MWNT) and acid functionalized (f-MWNT) were used and the respective CNT contents were restricted to 4wt% and 0.5wt% in composites, since high CNT content did not show large improvements in the EMI shielding properties.[32,33] The shielding properties are correlated with the dispersion of CNTs and the electrical conductivity of composites. The CNT dispersion and

local nanostructural conductivity of the composite films were investigated by scanning electron microscopy (SEM), transmission electron microscopy (TEM) and conducting-atomic force microscopy (C-AFM), respectively. The key objectives of the present study are: (a) to investigate the effect of functionalization of MWNTs on the EMI shielding properties of composites in the frequency range of 1-18 GHz, (b) to study the correlation between electrical conductivity and EMI shielding effectiveness and (c) to predict the shielding mechanisms in these composites by taking absorption and reflection losses into account.

2. EXPERIMENTAL

2.1. Materials and methods

Materials

An industrial grade MWNT (Grade 7100, outer diameter: ~13 nm) was purchased from Nanocyl, Belgium. PVDF (Kynar 720) pellets were obtained from Atofina, USA. Nitric acid (69%, analytical grade) was purchased from Thomas Baker, India. Silver paste was purchased from RS Components, Northants, UK. Deionized water (pH ~6.5) was used throughout the experiments.

Acid-functionalization of MWNT

One g of MWNTs was refluxed with a mixture of 200ml deionized water and 5ml of conc. HNO_3 at 90°C for 24 h. The MWNT suspension was filtered and washed several times with large amount of deionized water and thoroughly dried in vacuum oven at 85°C overnight. The resulting black powder was characterized by transmission electron microscopy (TEM), thermogravimetry analysis (TGA), Raman spectroscopy and FTIR and the results are presented in Supporting Information (SI). The functionalized CNT is denoted as f-MWNT.

Composite preparation

The composites were prepared by melt-mixing method using a Laboratory batch mixer (50 EHT 3Z, Brabender Plastograph, Germany), equipped with counter rotating screws of length 50 mm. The melt-mixing was carried out at ~200ºC for 5 min at a screw speed of 90 rpm. Prior to the composite preparation, PVDF beads were dried in vacuum at 80°C for 12 h. During mixing, the torque as a function of time was measured using a software (Plasti-Corder and mixer measuring head fusion Behavior/version 4.2.10). The results of torque vs. mixing time and torque values for various composites are presented in SI. The resulting composites were successively palletized.

About ~3-5g of samples were hot-pressed using hydraulic press (50ton, AHP-717, Achieve Hydraulics, India) between two stainless steel platens (250mm×250mm) with a load of 11 tons at ~180(±10)°C for ~10 min. The heating was carried out at ~1.2°C/min. The films were removed from the press at room temperature. The details of the various film samples prepared by the above method and their acronyms are presented in Table 1. For comparison, the neat PVDF film was also prepared by the same method. The thickness and diameter of the films were found to be ~0.3 (±0.015) mm and ~150 mm, respectively. The middle portions of the films, which had uniform thickness, were used for all the measurements. The schematic of the above mentioned process is shown in SI (Fig. S7).

Table 1. Weight percentage of fillers used in PVDF matrix for composite preparation and composite acronyms

S. No	Sample Details	MWNT content (wt. %)	Designation
1	Neat PVDF	0	PVDF
2	PVDF+uf-MWNT	0.1	0.1uf-MWNT
		0.2	0.2uf-MWNT
		0.35	0.35uf-MWNT
		0.5	0.5uf-MWNT
		1.7	1.7uf-MWNT
		3.15	3.15uf-MWNT
		4	4uf-MWNT
3	PVDF+f-MWNT	0.1	0.1f-MWNT

	0.15	0.15f-MWNT
	0.2	0.2f-MWNT
	0.25	0.25f-MWNT
	0.35	0.35f-MWNT
	0.5	0.5f-MWNT

2.2. Characterization

Dispersion of MWNTs in polymer matrix was investigated through fractographic studies by field emission scanning electron microscope (FESEM) (SIGMA, Carl Zeiss, Germany). The film samples were cryo-fractured in liquid nitrogen and subsequently coated with Au-Pd sputtering prior to imaging. Transmission electron microscopy (TEM) was carried out using high resolution microscope (G220S-Twin, Tecnai, FEI, USA). About 100 nm films were cut using ultra-microtomy (Leica EMFCS) and transferred onto Cu grids. Conducting-atomic force microscopy (C-AFM) (Asylum Research, USA) was carried out on compression moulded films to investigate the nanoscale dispersion of CNTs by studying the nano-structured electronic properties on the surface. The film samples were coated with silver paste on one side for the contact and mounted on to the sample stage for measurements and imaging. The current-voltage (I-V) characteristics of the composite surface was evaluated using C-AFM. In this technique, a silicon cantilever coated with chromium-gold tip was used and the imaging was carried out in contact mode at a resonance frequency of 75 KHz. The topographic images were obtained at zero bias voltage. The I-V curves were obtained in the the bias voltage between -2 and +2V. All the measurements were performed at room temperature and under ambient conditions. The AC electrical conductivity was measured on film samples at room temperature using a broadband impedance analyzer (Novocontrol Alpha-A, Germany) in the frequency between 10^{-1} and 10^{6} Hz. The films were cut in the diameter of 20 mm from compression moulded sheets and conducting electrodes were made using silver paste.

The EMI shielding properties were measured using a two-port Vector Network Analyser (VNA) (N5222A, 10MHz-26.5GHz, Agilent, USA) in the frequency range of 1 GHz to18 GHz. Calibration of the instrument and waveguides was carried out using open-short-load technique. The dimensions of the waveguides used were the following: 165.1 × 82.5 mm^2 for L band, 72.1 × 34.0 mm^2 for S band, 34.8 × 15.7 mm^2 for C band, 22.8 × 10.1 mm^2 for X band and 15.7 × 7.8 mm^2 for Ku band. Separate experiments were conducted for each band. The film samples were cut into the dimensions as per waveguides. The reflection (S_{11} or S_{22}) and transmission (S_{12} or S_{21}) coefficients or losses with frequency were recorded for all the samples. The total shielding effectiveness (SE_T) is computed using the following relationship: $SE_T = SE_R + SE_A + SE_M$, where $SE_R = 10\log(1 - |S_{11}|^2)$, $SE_A = 10\log\frac{(1-|S_{11}|^2)}{|S_{21}|^2}$ and SE_M are shielding effectiveness due to reflection , absoprtion and multiple reflections, respectively. If total SE is more than 10 dB, SE due to multiple reflections can be neglected and therefore the SE depends on SE due to reflection and absorption losses only.[20,50] The EM radiation blocking efficiency of a shield or the SE_T (in dB) is measured in terms of a logarithmic quantity and can be expressed as:[10,58]

$$SE_T = 10.\log(\frac{P_{in}}{P_{out}}) = 20.\log(\frac{E_{in}}{E_{out}}) = 20.\log(\frac{H_{in}}{H_{out}}) \quad (1)$$

Where P_{in} is the incident energy field, P_{out} is the transmitted energy field and similarly E_{in} and H_{in} are the root mean square (rms) of incident electric and magnetic field strengths and E_{out} and H_{out} are the rms transmitted electric and magnetic fields of the electromagnetic wave, respectively.

3. RESULTS AND DISCUSSIONS

3.1 Functionalization of CNTs

The acid-functionalization of MWNTs carried out in this study was gentle as compared to the previously reported studies[42,59] in order to retain the structural integrity and electrical properties

of CNTs. Indeed we found that these properties were retained upon acid-treatment as confirmed by TEM of individual CNTs (Fig. S2 in SI) and impedance studies of CNT pallets (Fig. S3 in SI), respectively. Moreover, this process is actually a purification process rather than acid-functionalization. However, the gentle acid-treatment resulted in attachment of few functional groups and imparted disorderness in CNT backbone as inferred from FTIR and Raman spectroscopy (Fig. S1 in SI), respectively. Further it was observed that the average diameter of MWNT has reduced from ~13 (±1.5) nm to ~9 (±0.9) nm by acid-treatment as obtained from TEM (Fig. S2 in SI). Though the reduction of CNT diameter was marginal; but consistent along the CNT length upon acid-treatment. This may be due to removal of catalysts. The presence of catalyst can be seen in TEM image of uf-MWNT (Fig. S2a in SI). Further, TGA (Fig. S2c in SI) of CNT shows that thermal stability of MWNTs improved; especially at higher temperatures (≥650°C) upon acid-treatment. This is likely due to absence of impurities and/or catalysts in acid-treated CNTs.

3.2 Dispersion of CNTs

Dispersion of CNTs in the polymer matrix determines the PT of the composite film thereby realizing its potential as EMI shielding material. Therefore, we have carried out several complementary techniques to ascertain the state of CNT dispersion.

Dispersion of CNTs was determined indirectly by torque measurements during composite preparation. The results are presented in SI (Fig. S4 and S5). While mixing; the maximum torque obtained for pure PVDF was ~31 Nm; while for composites, the maximum torque values were ~52 Nm and ~67 Nm for 0.5wt% f-MWNT and 4wt% uf-MWNT composites, respectively. After about 1 min of mixing, the torque values decreased marginally and remained constant thereafter;

irrespective of the CNT type and weight fraction, which indicates a uniform mixing without any thermal degradation of polymer.

Figure 1(a-d) present the typical FESEM images of 0.5uf-MWNT and 0.5f-MWNT composites. As expected, neat PVDF shows a featureless cryo-fractured surface (Figure not shown), however composites on the other hand show fibrous features on the surface, which are most likely due to the dispersed CNTs in the matrix or CNTs coated with the polymer matrix. Further it can be clearly seen that the fibrous structures are more prominent in 0.5f-MWNT composite (Fig. 1c, d) as compared to that in 0.5uf-MWNT (Fig. 1a, b). We measured the average diameters of MWNTs dispersed in PVDF in selected composites for comparison. The average diameter of CNTs in matrix are found to be ~33 (±3) nm and ~52 (±4) nm in case of 0.5uf-MWNT and 0.5f-MWNT composites, respectively. These higher values of diameter in comparison with that of CNT are most likely due to coating of CNTs by polymer chains by assuming dispersion of individual CNTs in polymer matrix. Further, the higher diameter of CNT in case of f-MWNT than that of uf-MWNT composites implies better interfacial adhesion between f-MWNTs and PVDF. Dispersion of f-MWNT in the matrix was studied by TEM. Figures 1e, f present bright field TEM images of 0.5f-MWCNT composite. The uniform dispersion of individual CNTs in PVDF matrix can clearly be seen in the image. At higher magnification, individual f-MWCNTs can be clearly seen in different regions (Figure 1f). These results are further corroborated by the impedance studies, where it was found that higher content of uf-MWNT was required to achieve PT as compared to that of f-MWNT in matrix, which are discussed in the subsequent section.

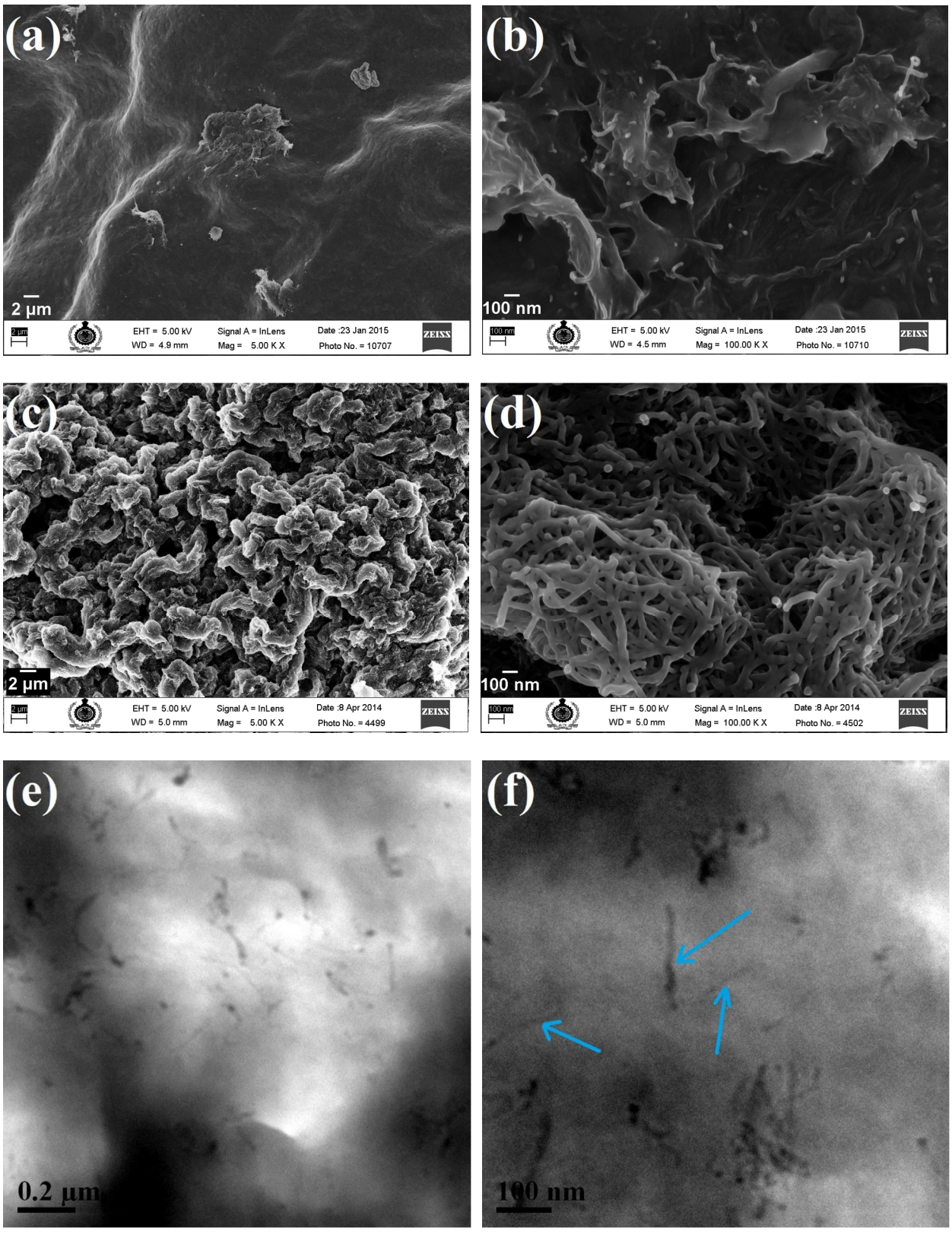

Figure 1. Cryo-fractured FESEM images of (a), (b) 0.5uf-MWNT; (c), (d) 0.5f-MWNT composites and (e), (f) bright field TEM images of 0.5f-MWNT composite film. The arrows show the individual CNTs.

3.3 Electrical conductivity and prediction of dispersion behavior

The room-temperature AC conductivity as a function of frequency for various samples are illustrated in Figure 2. As expected, the electrical conductivity increases with increase in CNT content (Figure 2a, b). Neat PVDF and composites with uf-MWNTs and f-MWNT up to 0.2wt% and 0.1wt%, respectively, showed an insulating behavior with conductivity values of ~10^{-13} to 10^{-12} S/cm at 0.1 Hz and the conductivity increased with frequency, which is a typical behavior of dielectric material.[60] In contrast, the composites with uf-MWNT contents of 0.35 and 0.5wt% showed about 4 to 5 orders increase in conductivity at 0.1Hz (from 10^{-12} S/cm for 0.2uf-MWNT to 10^{-7} S/cm for 0.5uf-MWNT). Further, in these two cases, the conductivity was found to be independent of frequency till ~10^{3} Hz, then it increased with frequency. This frequency-independent nature of composites is due to the polarization of dipoles, which dominate the DC conductivity.[61] Further at higher weight content of uf-MWNT (≥1.7wt%), the composites achieved conductivity values of about 10^{-4} to 10^{-3} S/cm and the values were independent of frequency throughout the studied range. The onset of frequency-independent behavior of CNT composites is considered as the transition from non-conducting to conducting nature.[29] Therefore, 0.35wt% was considered to be the PT for uf-MWNT. Similarly, for f-MWNT composites, the PT was found to be 0.15wt%. The significant lower PT in case of f-MWNT composites in comparison to uf-MWNT counterparts suggests better dispersion of f-MWNT than uf-MWNT in matrix. Better dispersion of CNTs in matrix leads to formation of three dimensional network structures due to the large aspect ratio of CNTs, which creates a continuous conducting path.[62] Further, in both the composites, above the PT, the conductivity values were

found to further increase with CNT content. This could be due to formation of multiple conducting paths of CNTs.[62] It was observed that in 3.15 and 4wt% uf-MWNT composites, the conductivity values decreased marginally with frequency between 10^5 and 10^6 Hz. This kind of behavior is not well understood; however, this could be likely due to agglomeration of CNTs at higher weight contents in polymer and skin affects at high frequencies. Similar behavior was recently reported by Guo et al.[63]

The DC conductivity (σ_{dc}) of the nanocomposites above PT can be explained using a power law[24,64] as given in eq 2.

$$\sigma_{dc} \propto (v - v_c)^e \qquad (2)$$

Where v is volume fraction of filler, v_c is critical volume fraction, and e is the critical exponent. The charge-transport mechanism in the composites can be explained using the AC universal law as given in eq 3.[26,65]

$$\sigma_{ac}(\omega) = \sigma_{dc}(0) + A(\omega)^e \qquad (3)$$

Where σ_{ac} is the AC conductivity, σ_{dc} is the DC conductivity independent of frequency, A and e are constants and, temperature and frequency dependent parameters, and $\omega\ (= 2\pi f)$ is the angular frequency.

The AC conductivity curves for 0.35uf-MWNT (Figure 2a) and 0.15f-MWNT (Figure 2b) can be divided into two regions: (i) the DC plateau in low frequency region (10^{-1}-10^3 Hz), (ii) frequency dependent region in high frequency region (10^3-10^6 Hz). The conductivity values obtained for composites above PT in both the cases are approximately equivalent to that for the CNT pallets, made from CNT compacted powder samples (~3.6×10^{-3} S/cm for both uf-MWNT and f-MWNT pallets) irrespective of the frequency studied, which again implies the CNT network formation. Note that these conductivity values of CNTs do not represent the inherent

conductivity of individual CNT, which is several order of magnitude higher than the values obtained here. This is mainly due to contact and constriction resistance of CNTs and also that of the instrument. This further indicates that the conductivity of CNTs was not affected much upon acid functionalization as the CNT pallets for both the cases were made by similar processes. The details of sample preparation and impedance studies for the various CNT pallets are presented in SI (Fig. S3). The PT obtained for f-MWNT (~0.15wt%) in the present study is lower than many previously reported studies[3,62,66-68].

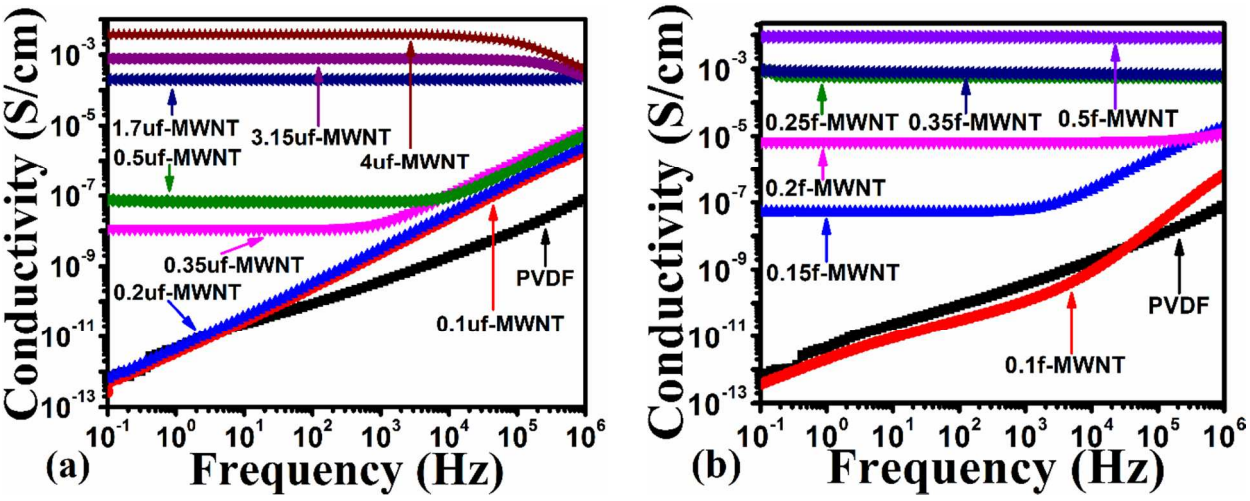

Figure 2. AC conductivity as a function of frequency for pure PVDF and various composites: (a) uf-MWNT and (b) f-MWNT.

3.4 Dispersion *via* AFM and C-AFM studies

The C-AFM technique was probably used for the first time for predicting the dispersion of CNTs in composites; besides investigating the I-V characteristics. We have carried out C-AFM measurements on 0.5f-MWNT and 0.5uf-MWNT composites in order to compare the state of dispersion of CNTs in these two cases. Figure 3a-b present the topographic AFM image and the corresponding current image for 0.5uf-MWNT, respectively and the corresponding images are shown in Figure 3c-d for 0.5f-MWNT composite films. Figure 3a presents the topographic

image of uf-MWNT composites. From this topography, the fibrous structure of CNTs cannot be observed clearly likely due to agglomeration. The corresponding C-AFM image is shown in Figure 3b, where it can be observed that uneven distribution of current by application of small bias voltage (-2 to +2V). At certain locations the local current yield reached to a high value (~5 nA) perhaps due to presence of high density of CNTs (indicated by the color code in Figure 3b); while the other regions do not show any current at all likely due to absence of CNTs at those locations. Due to the high localized current, the I-V characteristic curve could not be recorded for 0.5uf-MWNT. The high current yield at certain locations as seen in the present case is most likely due to tendency of pristine MWNTs to form agglomeration due to strong van der Waals forces between them.[69] In constrast to uf-MWNT, the fibrous structure of CNTs on the surface of f-MWNT composites can clearly be seen in Figure 3c. The C-AFM image (Figure 3d) for f-MWNT composites also showed a striking difference, when compared with that of uf-MWNT, in terms of current yield and its distribution. The current was found to be uniformly distributed on the film surface at low bias voltages (-2 to +2V), which indicates a good dispersion of f-MWNT on the film surface.

In order to obtain the local conductivity information in f-MWNT composites, the I-V curves were plotted with bias voltage between -2 and +2V on the regions where current is obtained (blue regions in Figure 3d). We found that the regions which looked dark in Figure 3d did not show any current in the I-V curve. The I-V curves were measured at about ten different locations on 0.5f-MWNT composite film and the average I-V curve in log-log is plotted in Figure 4, which shows a typical semiconducting nature.[70] As shown in Figure 4, the curve can be divided into two linear regions with slopes ~0.5 and ~2.4, which indicate two different electron transport regimes with a transition at ~0.16V. The power-law dependence of current on voltage

is given by $I \propto V^n$. The slope, n = 0.5, indicates electron transport by space-charge limited current (SCLC) and n = 2.4 (voltage>0.16V) indicates the trap-limited SCLC.[71]

A schematic representation of percolation of CNTs in polymer matrix for uf-MWNT and f-MWNT is presented in Figure 5. Due to agglomeration, bundles of uf-MWNTs are dispersed in matrix, which requires a higher amount of CNT content to make a conducting path in matrix in comparison to f-MWNT, which are individually dispersed in polymer matrix.

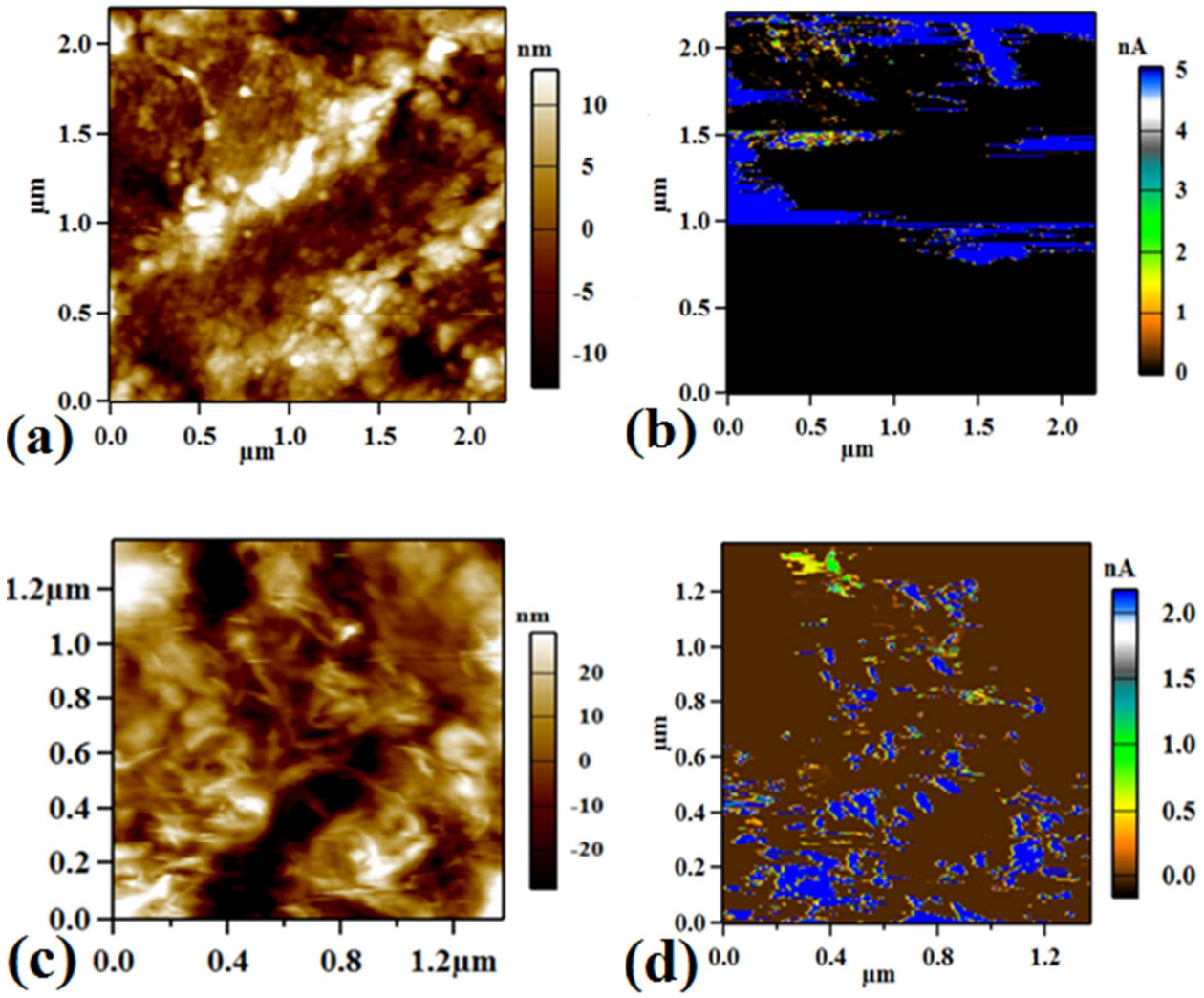

Figure 3. AFM and the corresponding C-AFM images of (a and b) uf-MWNT and (c and d) f-MWNT composite films. The measurements were performed by contact mode on compression molded films using Cr-Au coated Si tip.

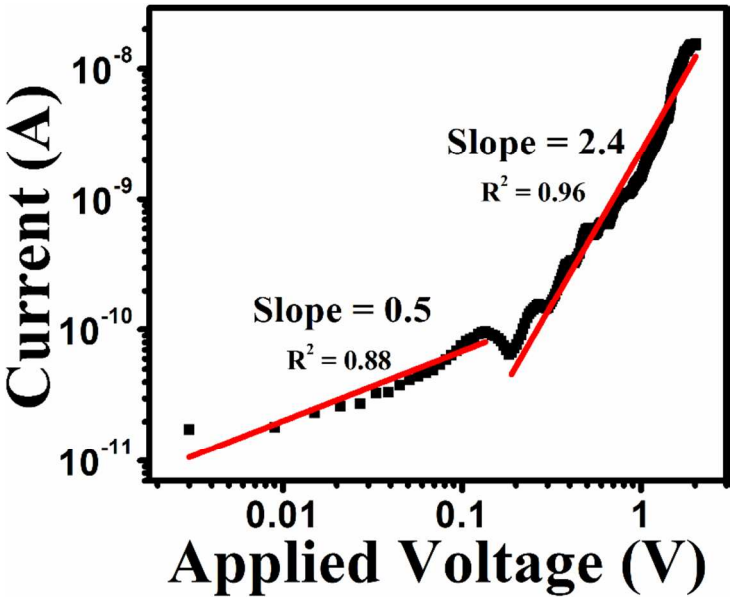

Figure. 4 The log-log plot of the I-V characteristics for 0.5f-MWNT composite film, measured in the blue regions of Fig. 3d.

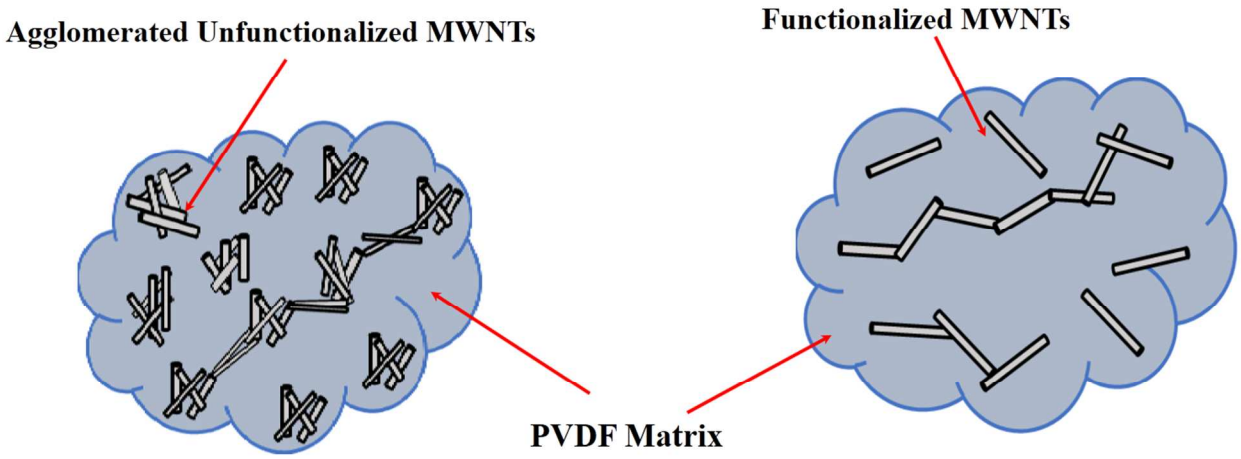

Figure 5. Schematic representation of conducting network of uf-MWNT (left) f-MWNT (right) in the PVDF matrix

3.5 EMI shielding effectiveness

It is important to mention that all the measurements were performed on the films of thickness ~0.3 (±0.015) mm, since shielding effectiveness is a thickness dependent property.[36] The SE_T vs. frequency curves for various EM bands for neat PVDF and uf-MWNT composites are presented

in Figure 6. The SE_T values showed frequency-dependent behavior in all the cases regardless of the bands studied. It can be seen that neat PVDF film showed average SE_T values between 1 dB and 8 dB in S, C, J and X bands; except for Ku band, where the SE_T was found to be highly frequency-dependent and showed the maximum peak values of ~12, ~11 and ~11 dB at 14, 15.4 and 17.1 GHz, respectively. For uf-MWNT composites, the SE_T for different bands: L, S, C, J, X and Ku are presented in Figure 6a-f, respectively. Interestingly, for L band, both neat PVDF and uf-MWNT composites irrespective of CNT content showed an SE_T of 80-100 dB at ~1 GHz (Fig. 6a), which is a quite significant value, even though in a very narrow frequency range, then the SE_T showed a progressive decrease with frequency. Considering the high SE values at ~1 GHz, repeatability of the results was checked at least once. The unprecedented SE_T value at low frequency (~1 GHz) exhibited by neat PVDF may be attributed to its intrinsic EM absorption properties.[42] The SE_T with frequency of uf-MWNT composites for S band is shown in Fig. 6b. The values were higher for initial frequency between 2.0 and 2.5 GHz; then the SE_T decreased and did not show much change with frequency. It was observed that there is a marginal "off-set" in the SE_T values (~13dB) particularly between L and S bands, which are low frequency bands. This is most likely due to experimental errors, since different waveguides were used for different bands.

The SE_T values for uf-MWNT composites in C, J, X and Ku bands showed a considerable variation with respective frequency ranges (Fig. 6c-f). This is likely due to the polarization effect and electrical losses in the samples particularly at higher frequencies.[72] This may also be related to frequency dependence behavior of permittivity of CNT composites as reported by Watts et al.[72] In Ku band, the SE_T showed a maximum variation with frequency. In L and S bands, the composites did not show any changes in the shielding properties up till 1.7wt%

uf-MWNT, however above this weight fraction the SE_T increased with CNT content till 4wt% uf-MWNT, which is the highest CNT content studied for this composites. Further, in C, J, X and Ku bands, the nature of the curves (SE_T vs. frequency) seems to be altered by incorporation of uf-MWNT; notwithstanding the weight fraction. The alternation is more pronounced in Ku band. This behavior is likely due to the interaction between EM waves with CNTs at higher frequencies. Furthermore, similar to L and S bands, in C, J and X bands, the SE_T increased from an average values of ~6, ~2 and ~1 dB for neat PVDF to ~12, ~8 and ~22 dB for 3.15wt% uf-MWNT and ~25, ~23 and ~53 dB for 4wt% uf-MWNT composites, respectively.

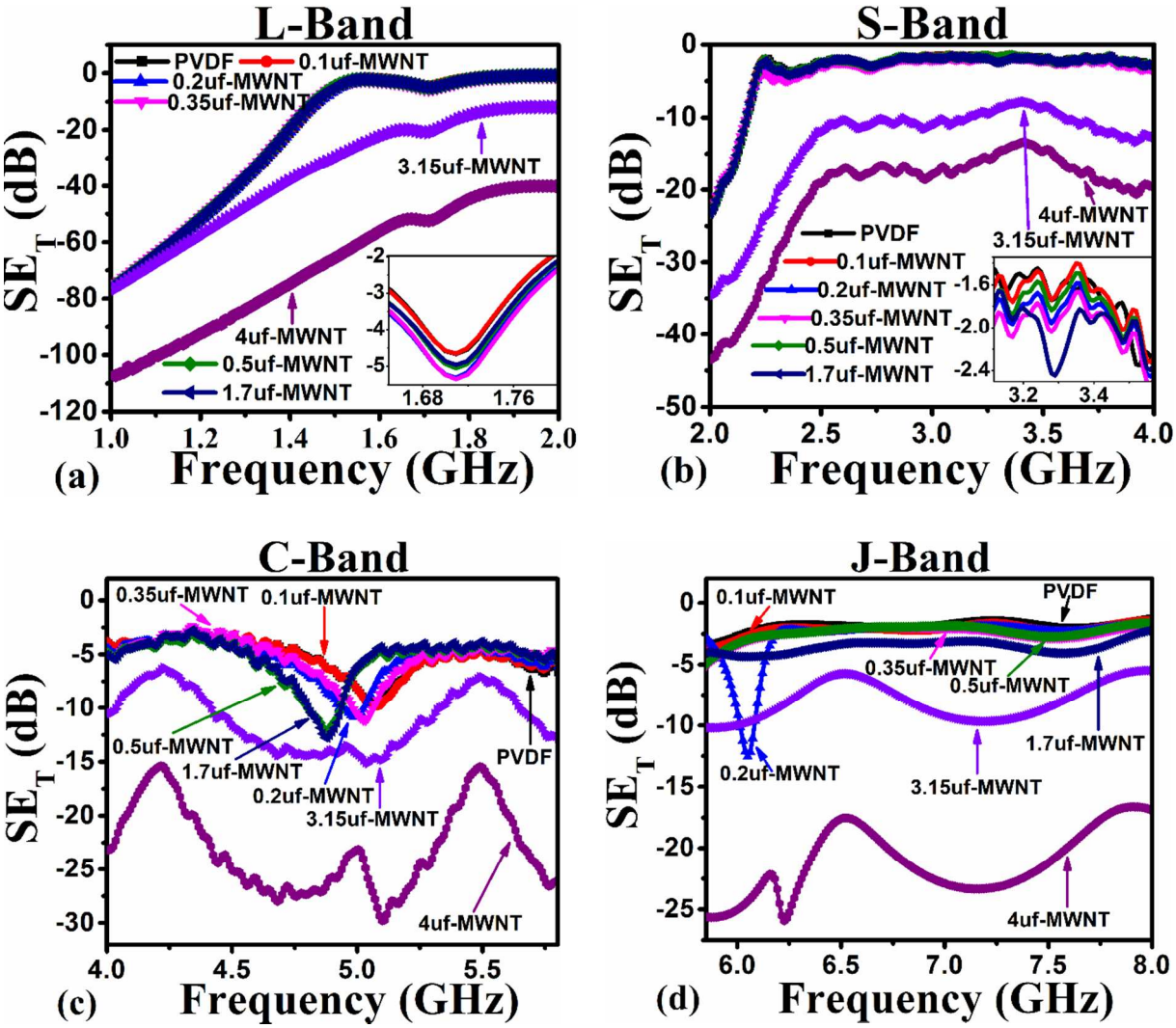

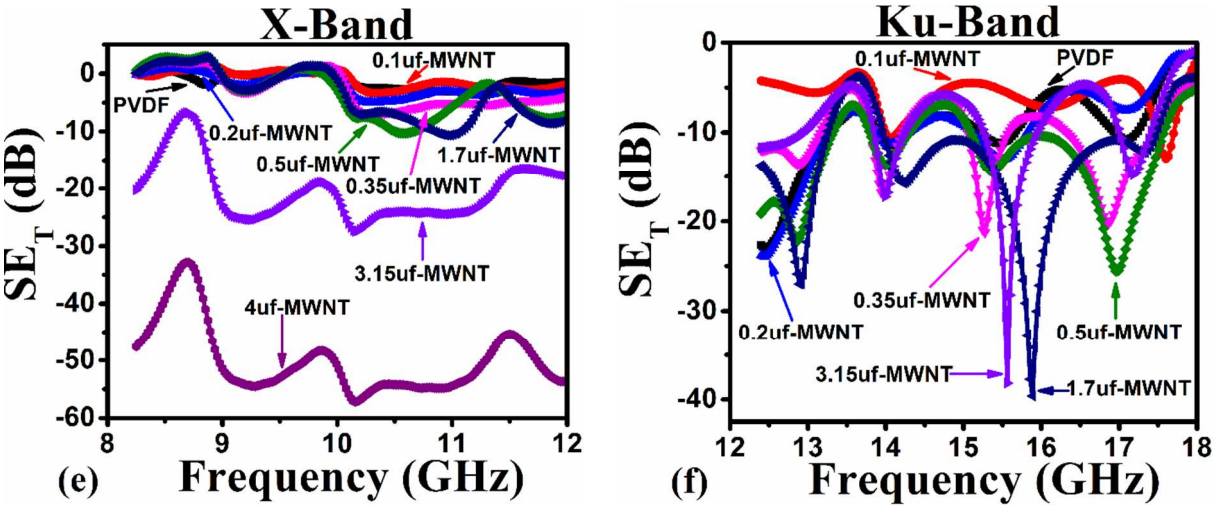

Figure 6. The SE_T as a function of frequency in (a) L, (b) S, (c) C, (d) J, (e) X and (f) Ku-bands for pure PVDF and uf-MWNT composites. The measurements are carried out on ~0.3 mm thick films for comparison.

Figure 7 presents the EMI SE behavior for f-MWNT composites as a function of frequency for various bands. Similar behavior of shielding effectiveness in all the bands as that in uf-MWNT composites was observed for f-MWNT composites as well. However, the difference is the CNT weight content, at which there is a significant increase in SE_T values. For uf-MWNT, this is 3.15wt%; whereas for f-MWNT; 0.5wt%. Up till 0.35wt% f-MWNT, the SE_T did not show any enhancement. However, the SE_T values increased significantly with 0.5wt% f-MWNT, which is the highest CNT content studied in these composites.

The maximum and average SE_T values for neat PVDF and selected composites which showed improvement in shielding properties are listed in Table 2. It can be seen that the EMI shielding values are different for different bands for a given sample, which is not clear. Further investigation is needed to understand this behavior. It is worth-noting that the maximum values obtained for 4wt% uf-MWNT composites are about 110, 45, 30, 26, 58 dB for L, S, C, J and X bands, respectively and the corresponding values for 0.5f-MWNT composites are about 98, 45, 26, 19, 47 dB. Here it is interesting to note that the SE_T values for 4wt% uf-MWNT are almost

comparable to that of 0.5wt% f-MWNT composites, which is apparently due to better dispersion of f-MWNT leading to formation of conducting network in the matrix. Further in both the composites, it was observed that the EMI SE properties showed enhancements in the composites which had CNT contents above their PT. To correlate the EMI shielding properties with that of electrical properties, both the average SE_T for various bands and the AC conductivity values at 1 KHz were plotted with CNT content in Figure 8 for uf-MWNT and f-MWNT composites. As seen in the figures, the average SE_T did not show much change in the values up to 1.7wt% and 0.35wt% in uf-MWNT (Figure 8a) and f-MWNT (Figure 8b) composites, respectively. The SE_T values only showed enhancements at ≥3.15wt% and at 0.5wt% of uf-MWNT and f-MWNT in composites, respectively; however as discussed earlier their corresponding PT values are 0.35wt% and 0.15wt%. Further, it was observed that the composites (4uf-MWNT and 0.5f-MWNT), whose conductivities are comparable (~10^{-3} S/cm) with each other, showed the maximum SE_T values, which are also comparable. Therefore, this plausibly indicates that there is a minimum conductivity requirement (perhaps ~10^{-3} S/cm) to achieve good EMI shielding properties. There may be another criterion for achieving good EMI shielding properties particularly in CNT or similar filler based composites as seen in the present case that the filler content should be well above the PT. Above PT, multiple conducting paths were created by CNT networks, which may help in attenuating the EM waves resulting in higher shielding properties.[73] This phenomenon is likely to help in designing future composites for EMI shielding.

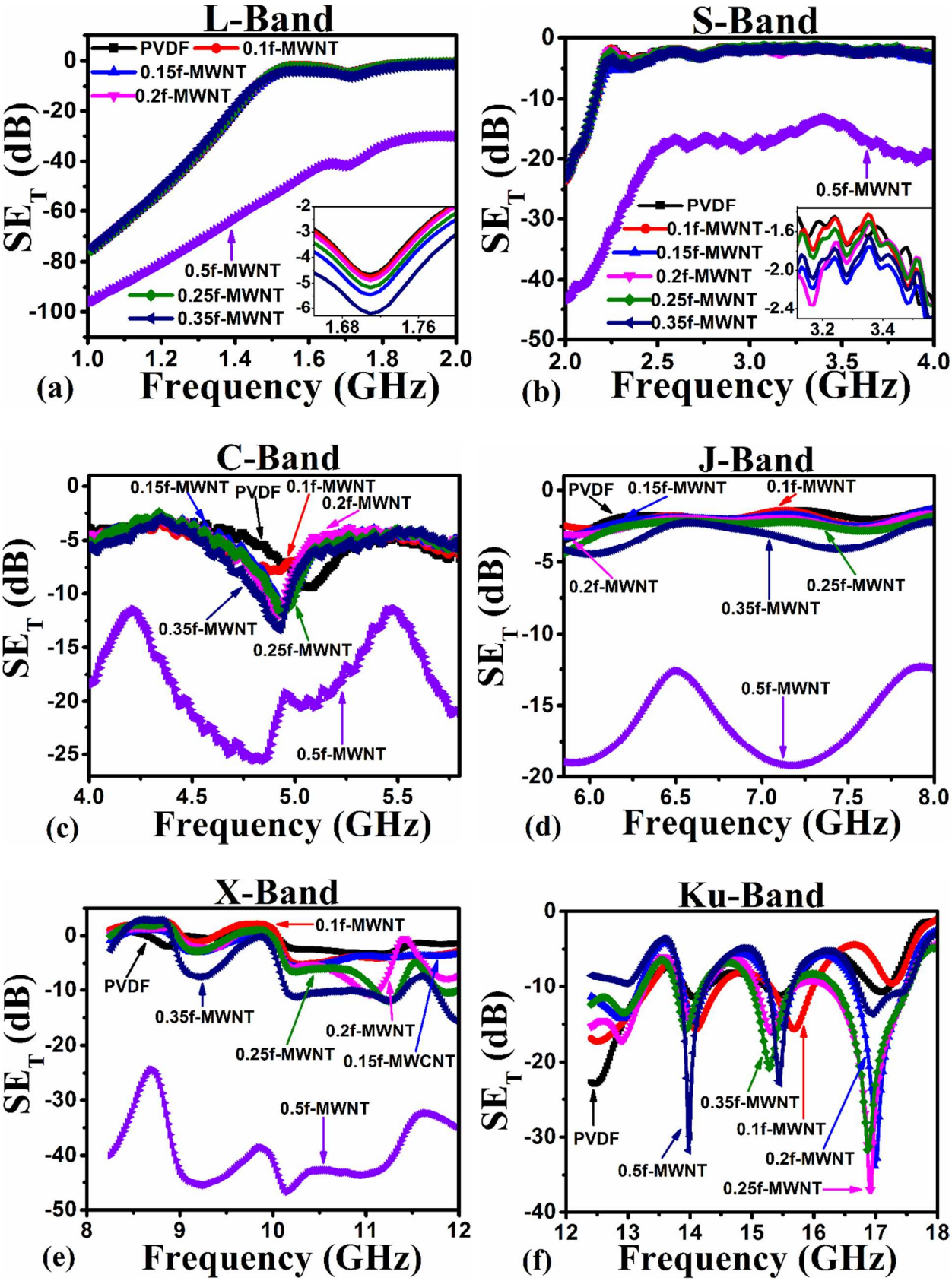

Figure 7. The SE_T as a function of frequency in (a) L, (b) S, (c) C, (d) J, (e) X and (f) Ku-bands for pure PVDF and f-MWNT composites. The measurements are carried out on ~0.3 mm thick films.

Table 2. The maximum and average SE_T values for PVDF and selected composites at different bands

	SE_T (dB) loss											
EM bands	L (1-2GHz)		S (2-4GHz)		C (4-5.8GHz)		J (5.8-8GHz)		X (8-12GHz)		Ku (12-18GHz)	
SE (dB)	Max	Avg	Max	Avg	Max	Avg	Max	Avg	Max	Avg	Max	Avg
Pure PVDF	75	30 (±20)	25	8(±4)	10	6(±1)	3	2(±0)	3	1(±1)	12	8(±4)
0.5f-MWNT	98	63(±20)	45	28(±7)	26	20(±4)	19	16(±2)	47	39(±5)	32	15(±4)
3.15uf-MWNT	77	42(±18)	35	19(±6)	15	12(±3)	10	8(±2)	28	22(±5)	38	18(±5)
4uf-MWNT	110	79(±20)	45	28(±7)	30	25(±4)	26	23(±3)	58	53(±6)	---	---

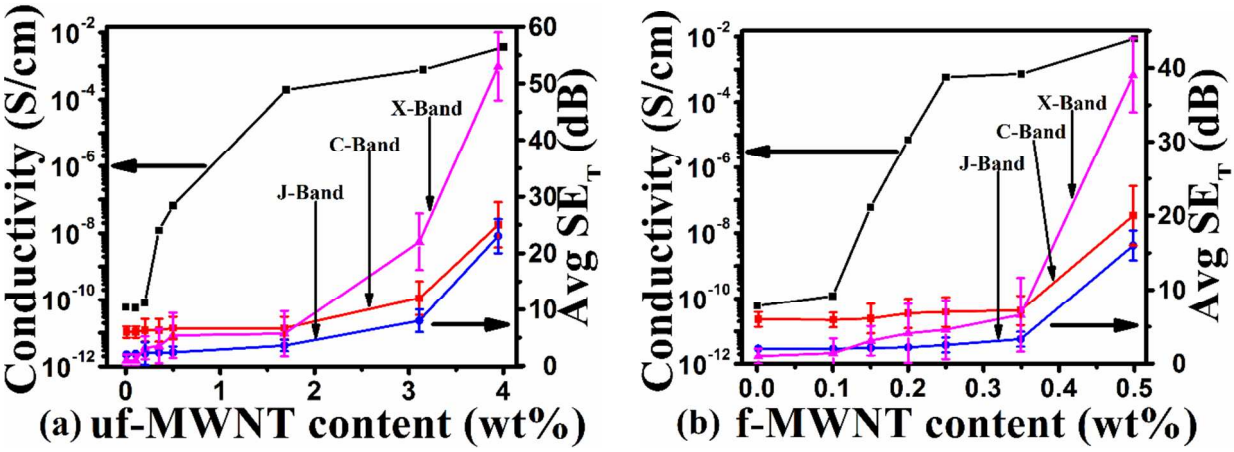

Figure 8. Electrical conductivity at 1 KHz and the average SE_T at different bands vs. weight fraction of (a) uf-MWNTs and (b) f-MWNTs.

To rationalize the discussion we compared our results with that of the reported in the literature and the data are comprehensively presented in Table 3. The EMI shielding for different frequency ranges for various polymer composites and the corresponding electrical conductivities are presented. It can be seen that the EMI shielding properties obtained in the present study is better than the studies mentioned in Table 3; except the work reported by Joshi et al,[50] considering the thickness and weight fraction of CNTs. Moreover, the present study reports a wide EM frequency range. A common finding, which can be drawn from Table 3 that the conductivity requirement for a good EMI shielding composite is ~10^{-4} S/cm or higher, which is

in agreement with the present study. Higher electrical conductivity signifies greater amount of nomadic charges that lead to enhanced EMI shielding.[9] Further, as discussed in the introduction section, the results in the present study accompanied with a critical analysis of Table 3 give an insight into why there is a significant scatter in the EMI shielding properties of polymer composites in the literature. As seen in the present case the electrical conductivities at the percolation threshold are ~10^{-8} and ~10^{-7} S/cm for uf-MWNT and f-MWNT composites, respectively. Such low values of conductivities may not be able to attenuate EM waves effectively, hence shielding properties were not found to improve in the composites even after attaining the PT, which is the onset of network formation. However, when the composites attained an electrical conductivity in the order of 10^{-3} S/cm well above their PT due to multiple conducting paths, the shielding properties improved significantly. Therefore, there seems a critical electrical conductivity, plausibly ~10^{-3} S/cm, above which the material acts as a good EMI shield.

Table 3. Comparison of EMI shielding properties obtained in the present study with that of the various polymer composites reported in the literature

Matrix	Filler	Preparation method	Filler conc. (wt%/vol%)	Thickness (mm)	σ (S/cm)	Max. SE (dB)	Frequency (GHz)	Ref
PS	MWNT	Melt mixing	20wt%	2	1	63	8.2-12.4	48
PS	CuNW	Melt mixing	2.1vol %	0.21	---	35	8.2-12.4	49
PES	Ni filaments	Melt mixing	7vol%	---	---	87	1-2	74
PET	CNT	Melt mixing	4wt%	2	---	18	7.6	75
PMMA	MWNT	Solution cast	10vol%	0.25-0.3	1.5	40	8.2-12.4	17
PANI	SWNT	Solution cast	25wt%	2.4	10	31	2-18	47
PANI	GS	Solution cast	33wt%	2.4	19	34	2-18	47
PANI	Y_2O_3	In-situ polymerization	20wt%	2.8	---	20	12.4-18	56
PP	CB	Melt mixing	10vol %	2.8	---	43	8–12.4	21
PC	MWNT	Melt mixing	5wt%	1.85	---	26	8.2-12.4	51
PTT	MWNT	Melt mixing	4.76vol%	2	$4x10^{-2}$	23	8.2-12.4	34
PVA	GNR	Solution cast	0.025wt%	0.6	10^{-2}	60	8.2-12.4	50
RET	CNT	Solution cast	3.2vol %	2	10^{-2}	28	8.2-12.4	52
PSU	CNFs	Solution cast	10wt%	1	$1.9x10^{-1}$	45	8.2-12.4	53
Varnish	CNT	Melt mixing	8wt%	1	---	24	15.3	75
PVDF foam	f-G	Solution cast	5wt%	---	10^{-2}	20	8-12	41
PVDF foam	f-G	Solution cast	5wt%	---	10^{-2}	18	1-8	41
PVDF	CuS	Solution cast	5wt%	3.5	---	102	7.7	43

PVDF	CNT	Solution cast	3wt%	1	10^{-3}	31	8-18	5
PVDF	CNT/BT-GO	Solution cast	3wt%/5vol%	1	10^{-4}	31	8-18	5
PVDF	CNT/CoNWs	Solution cast	3wt%/2.2vol%	1	10^{-3}	35	8-18	5
PVDF	IL-MWNTs	Melt mixing	2wt%	---	10^{-3}	20	8-18	40
PVDF	Activated CFs	Solution cast	40wt%	0.05	0.14	14	0.1-1	76
PVDF	BaTiO3-Ag	Solution cast	20vol%-10vol%	1.2	---	26	8.2-12.4	54
PVDF	carbonyl Fe powder	Solution cast	50vol %	1.2	0.12	20	8.2-12.4	55
PVDF	uf-MWNT	Melt mixing	4wt%	0.3(±0.015)	3.72×10^{-3}	~110	1-2	This work
						~45	2-4	
						~30	4-8	
						~58	8-12	
			3.15wt%	0.3(±0.015)	7.79×10^{-4}	~38	15.5	
PVDF	f-MWNTs	Melt mixing	0.5wt%	0.3(±0.015)	8.72×10^{-3}	~98	1-2	This work
						~45	2-4	
						~26	4-8	
						~47	8-12	
						~32	13.9	

[Abbreviations: PS: Polystyrene; PES: Polyethersulfone; PET: Poly(ethylene terephthalate); PMMA: Poly (methyl methacrylate); PANI: Polyaniline; PP: Polypropylene; PC: Polycarbonate; PTT: Poly(trimethylene terephthalate); PVA: Polyvinyl alcohol; RET: Reactive ethylene terpolymer; PSU: Polysulfone; GS: Graphene sheet; CB: Carbon black; GNR: Graphenenanoribbon; CNF: Carbon nanofibers; f-G: Functionalized graphene].

3.6 EMI shielding mechanism

In order to understand the shielding mechanism of composites we have used the absorption and reflection loss values at three different frequencies for each EM band and plotted against CNT weight fraction. The frequencies were chosen randomly at three almost equal intervals in the given EM band. Figure 9 presents the effect of uf-MWNT content on absorption (SE_A) and reflection (SE_R) losses of composites for various EM bands (Fig. 9a-f). It was observed that in all the bands the SE_A was found to be higher as compared to SE_R; notwithstanding the weight fraction of CNTs. Further, the SE_R was not affected much up to 1.7wt% of uf-MWNT in all the bands, except in Ku band; whereas the SE_A was not affected in L, S and C bands and only marginally increased in J, X bands. In Ku band, the SE_A values are random, but higher than SE_R. For composites with uf-MWNT ≥3.15wt%, both SE_A and SE_R showed increases with weight fractions of CNTs in all the bands except Ku band; however the SE_A was found to increase higher than that of SE_R with CNT content. For instance, the absorption loss for 4uf-MWNT

composites is ~49 dB; whereas reflection loss is only ~5 dB at 11 GHz (X band) (Fig. 9e). The average percentage contribution of absorption losses to shielding effectiveness for 3.15 and 4wt% uf-MWNT composites for various bands are ~83% and ~82%, respectively.

Similar results were obtained for f-MWNT composites as well for the same set of frequencies selected from the different EM bands; *viz.*, L, S, C, J, X and Ku and the corresponding absorption and reflection losses with CNT content are presented in Figure 10a-f, respectively. In composites up to 0.35wt% f-MWNT, the SE_R did not show any changes with CNT content in the bands studied. Similarly SE_A did not show changes in L, S bands; but for C, J, X and Ku bands it increased marginally with CNT content. However a significant increase in the SE_A is observed at only 0.5wt% f-MWNT composites for all the bands; except Ku, which is highly dependent on frequency. The average percentage contribution of absorption loss to shielding effectiveness for 0.5f-MWNT composites is found to be ~80%. For example, the SE_A and SE_R are ~38.4 dB and ~5 dB, respectively, at 11GHz (X band) for 0.5f-MWNT composites (Fig. 10e).

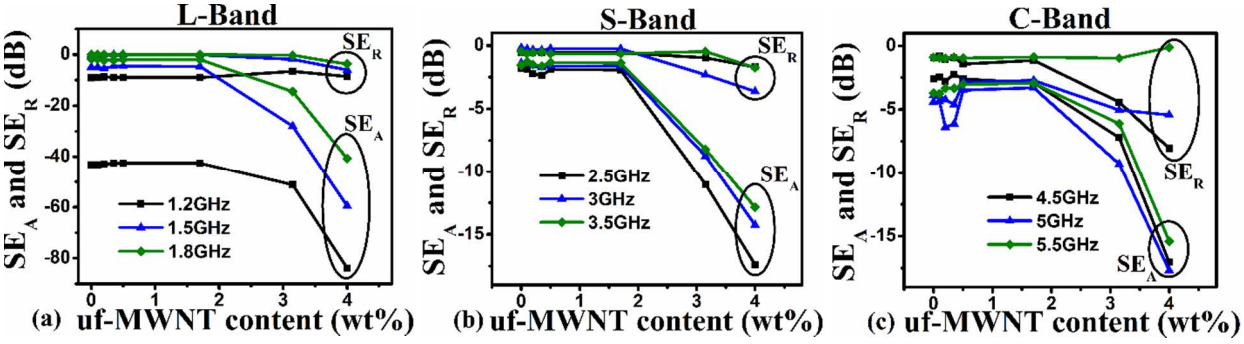

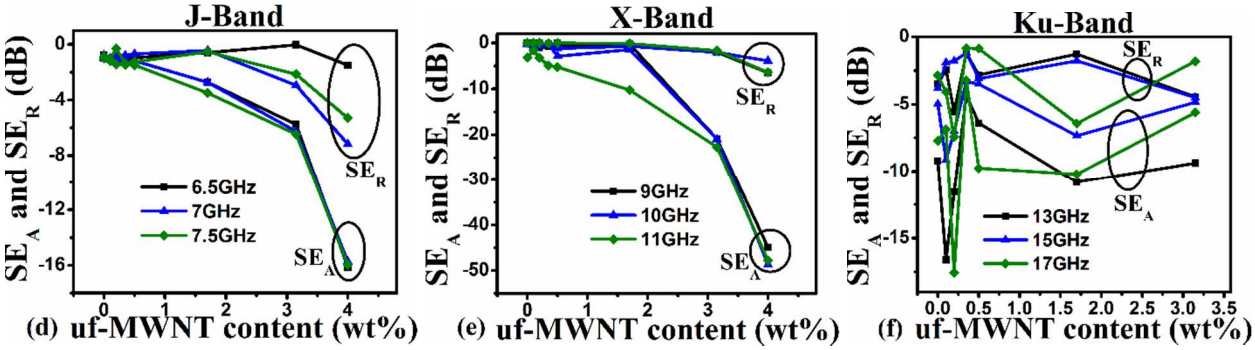

Figure 9. Contribution of reflection and absorption losses to shielding effectiveness of composites with uf-MWNT content for different frequency bands.

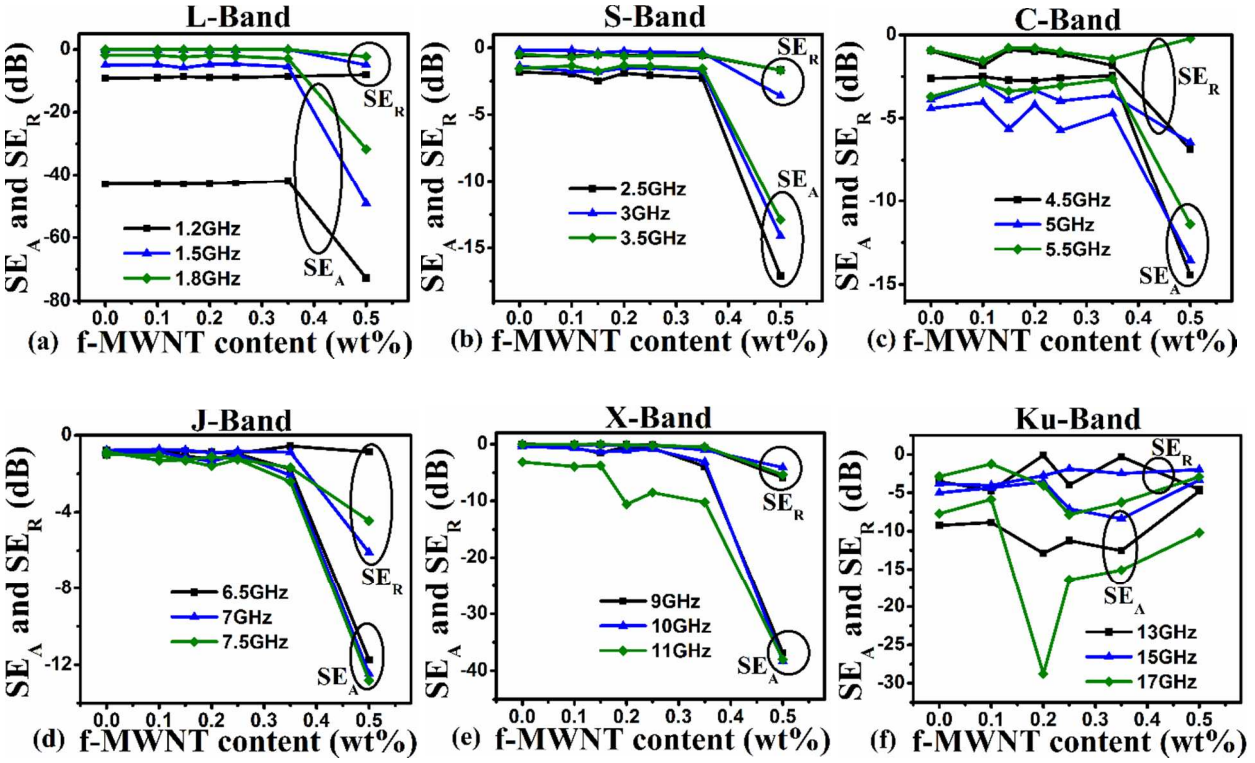

Figure 10. Contribution of reflection and absorption losses to shielding effectiveness of composites with f-MWNT content for different frequency bands.

On the basis of above results, it can be inferred that the primary shielding mechanism of PVDF/CNT composites is absorption with small contribution from reflection. This suggests that the composites in the present case are good EM absorbers. The SE_R and SE_A are related to the electrical conductivity of composites as given in eq 5 and 6, respectively.[50]

$$SE_R = -10\log_{10}\left(\frac{\sigma}{16\varepsilon\omega\mu}\right) \quad (5)$$

$$SE_A = -8.68t\left(\sqrt{\frac{\sigma\omega\mu}{2}}\right) \quad (6)$$

Where σ is electrical conductivity, ε is permitivity, ω is angular frequency, μ is magnetic permeability and t is thickness of the shielding material. From eq 5, a good EM reflecting material should have high electrical conductivity, low permitivity and magnetic permeability. From eq 6, a good absorbing material should possess high conductivity and high permeability for a given thickness. Further, it can be inferred from eq 5 and 6, that change in the absoprtion loss will be more pronounced than the reflection loss by change in electrical conductivity by assuming other properties to be invariant, which is validated in the present study. The composites which exhibited higher electrical conductivity showed higher absoprtion losses as well. This is further supported by the inherent EM absorbing properties of CNTs.[9] Good EM absorption properties are used in stealth technology.[73] The attenuation of EM waves via absorption is likely to produce heat in the shielding material and the heat is dissipated if the shielding material possesses a good thermal conductivity.[5] Moreover, CNT composites are reported to show better thermal conductivity as compared to neat polymer.[5]

4. CONCLUSIONS

We report excellent EMI shielding properties of PVDF-MWNT composites in different EM bands (L, S, C, J, X and Ku) at low acid-treated CNT content (0.5wt%). The maximum shielding effectiveness values for L, S, C, J, X and Ku bands are found to be ~98, 45, 26, 19, 47 and 32 dB, respectively. A method in which a dilute nitric acid-treatment of CNTs resulted in a significant improvement of their dispersion in matrix with a percolation threshold (PT) of 0.15wt%. The composites with CNT content well above its PT exhibited improved EMI

shielding properties likely due to multiple conducting paths. The EM waves are found to be attenuated by higher absorption loss than by reflection loss. The excellent EMI shielding properties of these composites in a wide frequency range pave the way for tailoring a versatile and lightweight EMI shielding material for various electrical and electronic, and for stealth applications. The latter application typically requires an EMI SE of more than 40 dB.

ASSOCIATED CONTENT

Supporting Information

Functinalization of MWNT results by FTIR, Raman, TGA and TEM images are presented in Figure S1 and S2. Impedance studies of MWNT pellets are presented in Figure S3. Torque measurements of PVDF and composites during melt-mixing are presented in Figure S4 and S5. Optical images of compression molded film samples are presented in Figure S6. Schematic diagram for PVDF composite preparation and characterization are presented in Figure S7. Graphical representation of EMI shielding is presented in Figure S8. FOM results of the composites are presented in Table S1. This material is available free of charge via the Internet at http://pubs.rsc.org.

AUTHOR INFORMATION

Corresponding Author

*Tel.: +91-20-24304309. Email: uma.patro@gmail.com; umasankarp@diat.ac.in

Notes

The authors declare no competing financial interest.

ACKNOWLEDGMENTS

TUP would like to thankfully acknowledge the funding from DST under Fast Track Project for Young Scientists (SB/FT/CS-043/2012). The authors are highly thankful to the financial supports

from DIAT (DU). The authors would like to thank Prof. Balasubramanian K., Dr. H. S. Panda, Dr. Vijay Hiwarkar and Mr. Radha Manohar Rao for technical discussion and support. The authors would also like to acknowledge the DRDO-DIAT program on Nanomaterials by ER-IPR, DRDO for providing various characterization techniques.

REFERENCES

(1) M. Imai, K. Akiyama, T. Tanaka and E. Sano, *Compos. Sci. Technol.*, 2010, **70**, 1564-1570.

(2) X. Jing, Y. Wang, and B. Zhang, *J. Appl. Polym. Sci.*, 2005, **98**, 2149-2156.

(3) V. Eswaraiah, V. Sankaranarayanan, and S. Ramaprabhu, *Nanoscale Res. Lett.*, 2011, **6**, 137.

(4) J. Arranz-Andres, N. Pulido-Gonzalez, P. Marin, A. M. Aragon and M. L. Cerrada, *Prog. Electromagn. Res. B*, 2013, **48**, 175-196.

(5) M. Sharma, M. P. Singh, C. Srivastava, G. Madras and S. Bose, *ACS Appl. Mater. Interfaces*, 2014, **6(23)**, 21151–21160.

(6) L. A. Belov, S. M. Smolskiy and V. N. Kochemasov, *Handbook of RF, Microwave, and Millimeter-wave Components*, Artech House, USA, 2012.

(7) W. Middleton and M. E. V. Valkenburg, *Reference Data for Engineers: Radio, Electronics, Computer, and Communications*, Newnes, USA, 2002.

(8) S. Kalia, *Springer Series on Polymer and Composite Material*, Springer, ISSN: 2364-1878.

(9) M. Chen, L. Zhang, S. Duan, S. Jing, H. Jiang, M. Luo and C. Li, *Nanoscale*, 2014, **6**, 3796.

(10) P. Saini, V. Choudhary, B. P. Singh, R. B. Mathur and S. K. Dhawan, *Mater. Chem. Phys.*, 2009, **113**, 919-926.

(11) S. S. Azim, A. Satheesh, K. K. Ramu, S. Ramu and G. Venkatachari, *Prog. Org. Coat.*, 2006, **55**, 1-4.

(12) R. Rohini and S. Bose, *ACS Appl. Mater. Interfaces*, 2014, **6(14)**, 11302-11310.

(13) D. Polley, A. Barman and R. K. Mitra, *Opt. Lett.*, 2014, **39**, 1541-1544.

(14) S. Pande, A. Chaudhary, D. Patel, B. P. Singh and R. B. Mathur, *RSC Adv.*, 2014, **4**, 13839-13849.

(15) Y. Li, C. Chen, S. Zhang, Y. Ni and Y. Huang, *Appl. Surf. Sci.*, 2008, **254**, 5766-5771.

(16) R. B. Mathur, S. Pande, B. P. Singh and T. L. Dhami, *Polym. Compos.*, 2008, **29**, 717-727.

(17) S. Pande, B. P. Singh, R. B. Mathur, T. L. Dhami, P. Saini and S. K. Dhawan, *Nanoscale Res. Lett.*, 2009, **4**, 327-334.

(18) Y. Li, C. Chen, J-T. Li, S. Zhang, Y. Ni, S. Cai and J. Huang, *Nanoscale Res. Lett.*, 2010, **5**, 1170-1176.

(19) Y. Yang, MC. Gupta, KL. Dudley and RW. Lawrence, *J. Nanosci. Nanotechnol.*, 2005, **5(6)**, 927-31.

(20) S. Maiti, N. K. Shrivastava, S. Suin and B. B. Khatua, *ACS Appl. Mater. Interfaces*, 2013, **5(11)**, 4712-4724.

(21) M. H. A. Saleh and U. Sundararaj, *J. Phys. D: Appl. Phys.*, 2013, **46**, 035304.

(22) M. H. A. Saleh, W. H. Saadeh and U. Sundararaj, *Carbon*, 2013, **60**, 146.

(23) R. Ravati, S. Yahud and M. S. A. Majid, *Appl. Mech. Mater.*, 2014, **554**, 145-149.

(24) L. Nayak, T. K. Chaki and D. Khastgir, *J. Appl. Polym. Sci.*, 2014, **131(24)**, 40914.

(25) Y. Su, B. Zhou, L. Liu, J. Lian, G. Li and G. Li, *Polym. Compos.*, 2014, **36(5)**, 23012.

(26) SC. Tjong, *J. Nanosci. Nanotechnol.*, 2014, **14(2)**, 1154-68.

(27) W-L. Song, M-S. Cao, M-M. Lu, S. Bi, C-Y. Wang, J. Liu, J. Yuan and L-J. Fan, *Carbon*, 2014, **66**, 67-76.

(28) S. Barrau, P. Demont, A. Peigney, C. Laurent and C. Lacabanne, *Macromol.*, 2003, **36**, 5187-5194.

(29) P. Saini, V. Choudhary, B. P. Singh, R. B. Mathur and S. K. Dhawan, *Synt. Met.*, 2011, **161**, 1522-1526.

(30) M. H. A. Saleh, and U. Sundararaj, *Carbon*, 2009, **47**, 1738-1746.

(31) Y. Yang, MC. Gupta, KL. Dudley and RW. Lawrence, *NanoLett*., 2005, **5(11)**, 2131-4.

(32) Z. Liu, G. Bai, Y. Huang, Y. Ma, F. Du, F. Li, T. Guo and Y. Chen, *Carbon*, 2007, **45**, 821-827.

(33) H. M. Kim, K. Kim, C. Y. Lee, J. Joo, S. J. Cho, H. S. Yoon, D. A. Pejaković, J. W. Yoo and A. J. Epstein, *Appl. Phys. Lett.*, 2004, **84**, 589-591.

(34) A. Gupta and V. Choudhary, *J. Mater. Sci.*, 2011, **46**, 6416-6423.

(35) W-K. Choi, M-S. Hong, H-S. Lee, K-Y. An, J-H. Bang, Y. S. Lee, and B-J. Kim, *Bull. Korean Chem. Soc.*, 2014, **35**, 597.

(36) C-S. Zhang, Q-Q. Ni, S-Y. Fu and K. Kurashiki, *Compos. Sci. Technol.*, 2007, **67**, 2973-2980.

(37) W-S. Jou, H-Z. Cheng and C-F. Hsu, *J. Alloys. Comp*., 2007, **434-435**, 641-645.

(38) Y. J. Kim, K. J. An, K. S. Suh, H-D. Choi, J. H. Kwon, Y-C. Chung, W. N. Kim, A-K. Lee, C J-I. hoi and H. G. Yoon, *IEEE T. Electromagn. C.*, 2005, **47**, 872.

(39) A. Gupta and V. Choudhary, *Compos. Sci. Technol.*, 2011, **71**, 1563-1568.

(40) M. Sharma, K. Sharma, J. Abraham, S. Thomas, G. Madras and S. Bose, *Mater. Res. Express.*, 2014, **1**, 035003.

(41) V. Eswaraiah, V. Sankaranarayana and S. Ramaprabhu, *Macromol. Mater. Eng.*, 2011, **296**, 894-898.

(42) S. K. Rath, S. Dubey, G. S. Kumar, S. Kumar, A. K. Patra, J. Bahadur, A. K. Singh, G. Harikrishnan and T. U. Patro, *J. Mater. Sci.*, 2014, **49**, 103-113.

(43) S. He, G-S. Wang, C. Lu, J. Liu, B. Wen, H. Liu, L. Guo and M-S. Cao, *J. Mater. Chem. A*, 2013, **1**, 4685.

(44) Z. Jia, Z. Wang, C. Xu, J. Liang, B. Wei, D. Wu and S. Zhu, *Mater. Sci. Eng. A*, 1999, **271**, 395-400.

(45) J. Nina and M. Sebastian, *Mater. Lett.*, 2013, **90**, 64-67.

(46) V. Bhingardive, M. Sharma, S. Suwas, G. Madras and S. Bose, *RSC Adv.*, 2015, **5**, 35909-35916.

(47) B. Yuan, L. Yu, L. Sheng, K. An and X. Zhao, *J. Phys. D: Appl. Phys.*, 2012, **45**, 235108.

(48) M. Arjmand, T. Apperley, M. Okoniewski and U. Sundararaj, *Carbon*, 2012, **50**, 5126-5134.

(49) M. H. A. Saleh, G. A. Gelves and U. Sundararaj, *Composites, Part A*, 2011, **42**, 92-97.

(50) A. Joshi, A. Bajaj, R. Singh, P. S. Alegaonkar, K. Balasubramanian and S. Datar, *Nanotechnology*, 2013, **24**, 455705.

(51) M. Arjmand, M. Mahmoodi, G. A. Gelves, S. Park and U. Sundararaj, *Carbon*, 2011, **49**, 3430-3440.

(52) S-H. Park, P. T. Theilmann, P. M. Asbeck and P. R. Bandaru, *IEEE T. Nanotechnol.*, 2009, **9(4)**, 464-469.

(53) L. Nayak, D. Khastgir and T. K. Chaki, *J. Mater. Sci.*, 2013, **48**, 1492-1502.

(54) N. Joseph, S. K. Singh, R. K. Sirugudu, V. R. K. Murthy, S. Ananthakumar and M. T. Sebastian, *Mater. Res. Bull.*, 2013, **48**, 1681-1687.

(55) N. Joseph and M. T. Sebastian, *Mater. Lett.*, 2013, **90**, 64-67.

(56) M. Faisal and S. Khasim, *Polym. Sci., Ser. A*, 2014, **56**, 366-372.

(57) L-L. Wang, B-K. Tay, K-Y. See, Z. Sun, L-K. Tan and D. Lua, *Carbon*, 2009, **47**, 1905-1910.

(58) P. Saini, and V. Choudhary, *J. Mater. Sci.*, 2013, **48**, 797-804.

(59) S. B. Park, M. S. Lee and M. Park, *Carbon Letters*, 2014, **15(2)**, 117-124.

(60) E. E. Shafee, M. E. Gamal and M. Isa, *J. Polym. Res.*, 2012, **19**, 9805.

(61) R. V. Barde, K. R. Nemade and S. A. Waghuley, *JAsCerS*, 2015, **3**, 116-122.

(62) W. Bauhofer and J. Z. Kovacs, *Compos. Sci. Technol.*, 2009, **69**, 1486-1498.

(63) Q. Guo, Q. Xue, J. Sun, M. Dong, F. Xia and Z. Zhang, *Nanoscale*, 2015, **7**, 3660.

(64) S. Kirkpatrick, *Rev. Mod. Phys.*, 1973, **45**, 574.

(65) G. C. Psarras, *Composite, Part A*, 2006, **37**, 1545-1553.

(66) D-X. Yan, K. Dai, Z-D. Xiang, Z-M. Li, X. Ji and W-Q. Zhang, *J. Appl. Polym. Sci.*, 2011, **120**, 3014-3019.

(67) A. Vavouliotis, E. Fiamegou, P. Karapappas, G. C. Psarras and V. Kostopoulos, *Polym. Comp.*, 2010, **31**, 1874-1880.

(68) J. K. W. Sandler, J. E. Kirk, I. A. Kinloch, M. S. P. Shaffer and A. H. Windle, *Polymer*, 2003, **44(19)**, 5893-5899.

(69) R. Gangopadhyay and A. De, *Handbook of Organic-Inorganic Hybrid Materials and Nanocomposites, Chapter H-Conducting Polymer Nanocomposites*, American Scientific Publishers, 2003.

(70) L. Zhang, T. Sakai, N. Sakuma, T. Ono and K. Nakayama, *Appl. Phys. Lett.*, 1999, **75**, 3527.

(71) J. Alvarez, I. Ngo, M-E. Gueunier-Farret, J-P. Kleider, L. Yu, P. R. Cabarrocas, S. Perraud, E. Rouvière, C. Celle, C. Mouchet and J-P. Simonato, *Nanoscale Res. Lett.*, 2011, **6**, 110.

(72) P. C. P. Watts, D. R. Ponnampalam, W. K. Hsu, A. Barnes and B. Chambers, *Chem. Phys. Lett.*, 2003, **378**, 609-614.

(73) J-M. Thomassin, C. Jerome, T. Pardoen, C. Bailly, I. Huynen and C. Detrembleur, *Mater. Sci. Eng. R*, 2013, **74(7)**, 211-232.

(74) X. Shui and D. Chung, *J. Electron. Mater*., 1997, **26**, 928-934.

(75) Z. Fan, G. Luo, Z. Zhang, L. Zhou and F. Wei, *Mater. Sci. Eng. B*, 2006, **132**, 85-89.

(76) B. O. Lee, W. J. Woo, H. S. Park, H. S. Hahm, J. P. Wu and M. S. Kim, *J. Mater. Sci.*, 2002, **37**, 1839-1843.

TABLE OF CONTENTS

FIGURES

"Figure 1. Cryo-fractured FESEM images of (a), (b) 0.5uf-MWNT; (c), (d) 0.5f-MWNT composites and (e), (f) bright field TEM images of 0.5f-MWNT composite film. The arrows show the individual CNTs"

"Figure 2. AC conductivity as a function of frequency for pure PVDF and various composites: (a) uf-MWNT and (b) f-MWNT"

"Figure 3. AFM and the corresponding C-AFM images of (a and b) uf-MWNT and (c and d) f-MWNT composite films. The measurements were performed by contact mode on compression molded films using Cr-Au coated Si tip"

"Figure. 4 The log-log plot of the I-V characteristics for 0.5f-MWNT composite film, measured in the blue regions of Fig. 3d"

"Figure 5. Schematic representation of conducting network of uf-MWNT (left) f-MWNT (right) in the PVDF matrix"

"Figure 6. The SE_T as a function of frequency in (a) L, (b) S, (c) C, (d) J, (e) X and (f) Ku-bands for pure PVDF and uf-MWNT composites. The measurements are carried out on ~0.3 mm thick films for comparison"

"Figure 7. The SE_T as a function of frequency in (a) L, (b) S, (c) C, (d) J, (e) X and (f) Ku-bands for pure PVDF and f-MWNT composites. The measurements are carried out on ~0.3 mm thick films"

"Figure 8. Electrical conductivity at 1 KHz and the average SE_T at different bands vs. weight fraction of (a) uf-MWNTs and (b) f-MWNTs"

"Figure 9. Contribution of reflection and absorption losses to shielding effectiveness of composites with uf-MWNT content for different frequency band"

"Figure 10. Contribution of reflection and absorption losses to shielding effectiveness of composites with f-MWNT content for different frequency bands"

TABLES

"Table 1. Weight percentage of fillers used in PVDF matrix for composite preparation and composite acronyms"

"Table 2. The maximum and average SE_T values for PVDF and selected composites at different bands"

"Table 3. Comparison of EMI shielding properties obtained in the present study with that of the various polymer composites reported in the literature"

TABLE OF CONTENTS/ABSTRACT GRAPHIC

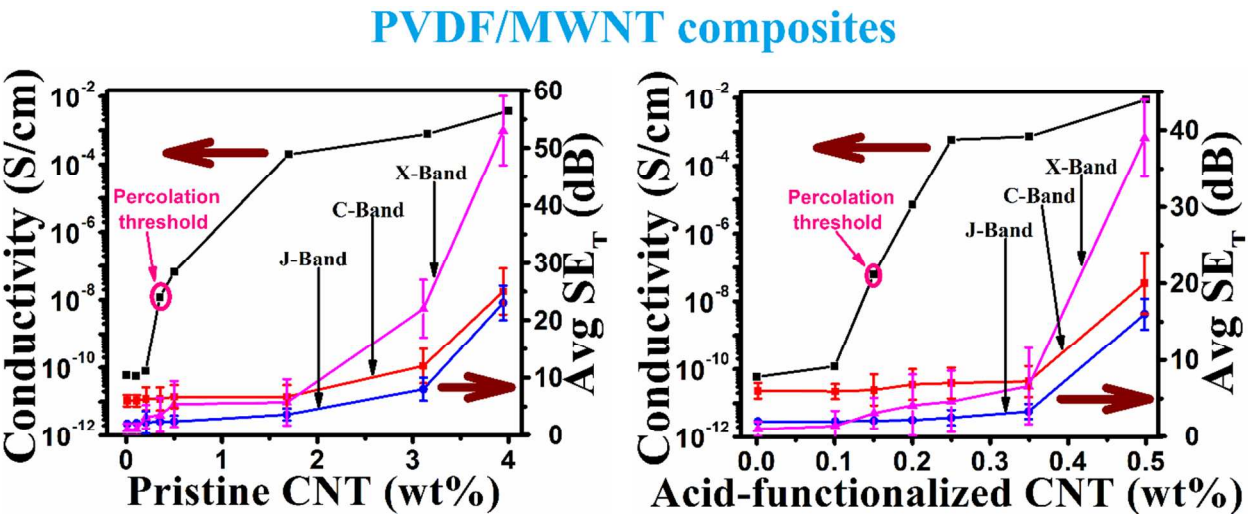

A dilute acid-treatment of MWNT showed a low electrical percolation in PVDF and significant improvements in EMI shielding properties.